PHYSICAL REVIEW B **93**, 035139 (2016)

$Cd_2Re_2O_7$ under high pressure: Pyrochlore lattice distortion-driven metal-to-nonmetal transition

Pallavi S. Malavi, S. Karmakar,[*] and S. M. Sharma
High Pressure and Synchrotron Radiation Physics Division, Bhabha Atomic Research Centre, Trombay, Mumbai 400085, India

(Received 1 November 2015; revised manuscript received 17 December 2015; published 28 January 2016)

Pyrochlore $Cd_2Re_2O_7$ has been investigated under high pressure by x-ray diffraction, resistivity and, mid-IR reflectance measurements. At ~14 GPa, the high-temperature cubic pyrochlore phase [space group (SG): $Fd\bar{3}m$] undergoes a second-order transition to a rhombohedral structure (SG: $R\bar{3}m$) with trigonal distortion in its pyrochlore lattice. Temperature-dependent resistivity $\rho(T)$ reveals a large number of exotic electronic phases (including superconducting and unconventional metallic phases) in its P-T phase diagram. At the metal-nonmetal boundary (at 21 GPa) the resistivity displays quadratic power-law behavior over a wide T range with possible formation of heavy mass coherent quasiparticles. In the nonmetallic state ($d\rho/dT < 0$), the nondivergent and quadratic power-law resistivity as $T \to 0$ reveals the novel character of the ground state. High-pressure optical conductivity measurement evidences electronic correlation playing the vital role in the emergence of the nonmetallic state as the electron-lattice coupling exceeds spin-orbit interaction due to large structural distortion.

DOI: 10.1103/PhysRevB.93.035139

I. INTRODUCTION

In heavy transition metal-based ($4d/5d$) oxides, the rather spatially extended nature of $4d/5d$ orbitals compared to $3d$ orbitals causes weaker on-site Coulomb correlation, making the spin-orbit interaction the dominant interaction energy scale [1,2]. Pyrochlore $A_2B_2O_7$ compounds, where B is a tetravalent or pentavalent transition metal ion and A, therefore, trivalent or divalent, respectively, are expected to be even more interesting due to the presence of geometrical frustration resulting in unusual magnetic ground states [3,4]. The strong interplay between spin-orbit interaction and electron correlation in the presence of crystal field interaction (due to ligand distortion of the BO_6 octahedra and/or anisotropic A-atom coordination) or electron-lattice coupling (pyrochlore lattice distortion) has recently been predicted to reveal novel ground states with exotic physical properties [5–9]. In real crystals the natural ligand distortions in the cubic pyrochlore lattice arise due to different A-atom sizes, whereas thermally driven structural transitions cause large electron-lattice coupling by removing geometrical frustration. The $4d/5d$ pyrochlore compounds with partially filled t_{2g} systems viz., ruthanate, iridate, osmate, and rhenate thus emerge in various novel phases and undergo metal-insulator, metal-semimetal, or superconducting transitions accompanying subtle or no structural transition, with or without emergence of magnetic ordering [10–13].

Among various $5d$ pyrochlores, $A_2Ir_2O_7$ compounds with Ir^{4+} in t_{2g}^5 electronic configuration have recently been studied extensively both by theory and experiments, because of their simple single-particle (hole) description ($J_{\text{eff}} = 1/2$). These are predicted to show various novel topological Mott insulating ground states as a function of the relative strength of crystal field, Coulomb correlation, and spin-orbit interaction [14]. As hydrostatic pressure can easily tune the above parameters along with the variation in d-orbital bandwidth by structural modifications without inducing disorder, pressure study is considered as a powerful tool to explore many such novel phases. Although some of these iridate compounds have revealed unconventional metallic phases by suppression of metal-to-insulator transition (MIT) [15,16], pyrochlore lattice distortion-driven stabilization of an insulating state with possible nontrivial surface state topology is yet to be experimentally verified.

Pyrochlore $Cd_2Os_2O_7$ with Os^{5+} in t_{2g}^3 electronic configuration has recently been found to show a novel magnetic insulating state originating from the large ligand distortion and competitive long-range anisotropic interaction below a Lifshitz-type MIT in its cubic pyrochlore phase [17–20]. Although no detailed high-pressure studies are reported so far, a moderate hydrostatic pressure up to 2 GPa is found to suppress the MIT and thus stabilizes the high-temperature heavy mass correlated metallic state [12]. On the other hand, pyrochlore $Cd_2Re_2O_7$ that possesses a very unconventional thermal transport and thermodynamic behavior above room temperature [21], exhibits a sharp transition in its metallic character accompanied by a cubic to tetragonal structural transition at $T_{s1} \sim 200$ K [22]. This is followed by another tetragonal structural transition at $T_{s2} \sim 120$ K and eventually undergoes a superconducting transition at ~1 K [13,23]. Upon increasing pressure, the bad metallic cubic pyrochlore phase with large geometrical frustration is stabilized by suppression of the above structural transitions [24–26]. There is evidence of strong electronic correlation in Re t_{2g} bands and enhanced Pauli susceptibility in this phase [27]. Thus both $Cd_2Os_2O_7$ and $Cd_2Re_2O_7$ are found to be suitable candidates to study the effect of pyrochlore lattice distortion on the metallic properties by high-pressure investigations. In this regard, $Cd_2Re_2O_7$ pyrochlore is of particular interest due to the t_{2g}^2 electronic configuration of the Re^{5+} ion. The local Coulomb interaction (Hund's coupling) in this system plays an important role along with the strong spin-orbit interaction in determining the local spin and orbital structure to emerge novel ground states. Another important parameter in $Cd_2Re_2O_7$ is the possible charge fluctuation in its pyrochlore lattice [23,28] due to rather unusual oxidation state of Re^{5+} ion, where lattice distortion may induce charge ordered state or a charge density wave (CDW) transition [5].

---

[*] sdak@barc.gov.in

As per the theoretical model suggested by Guo and Franz [6], pyrochlore lattice distortions along the [111] direction may be important for the realization of the topological insulator. Here we report the results of our first high-pressure electrical resistivity measurements up to 29 GPa in the temperature range 1.4–300 K on the [111] surface of a $Cd_2Re_2O_7$ pyrochlore crystal to study the effect of lattice distortion on the metallic state. The metallic resistivity shows dramatic changes in its temperature dependence at 21 GPa before undergoing transition to a nonmetallic state having weak negative temperature coefficient at $P > 24$ GPa. In order to gain insight of the corresponding lattice and electronic structural evolution, combined x-ray diffraction and midinfrared (MIR) reflectance measurements have been performed at room temperature up to 50 GPa and 37 GPa, respectively. The cubic pyrochlore lattice [$Fd\bar{3}m$] undergoes a second-order transition to a rhombohedral structure [$R\bar{3}m$] at ∼14 GPa. A drastic change in optical conductivity spectra with large suppression of incoherent Drude spectral weight (SW) across the metal-nonmetal transition suggests the possible formation of coherent quasiparticles in the nonmetallic state. A strong quasiparticle correlation can thus explain the observed unconventional transport behavior (Fermi-liquid resistivity at $T \rightarrow 0$) in this nonmetallic exotic ground state.

II. EXPERIMENTAL METHODS

Large single crystals of $Cd_2Re_2O_7$ were grown using a vapor transport technique, as described elsewhere [13]. Stoichiometric mixtures of CdO, Re, and ReO_3 were sealed in an evacuated quartz tube and heated at 900 °C for three days. The phase purity of the crystals was checked with powder x-ray diffraction. Our observed ambient pressure resistivity showing large residual resistance ratio ($\rho_{300K}/\rho_{5K} \sim 18$) and magnetic susceptibility data agree quite well with the reported results [13], supporting good quality of the crystal. Superconductivity with $T_c \sim 1$ K has been detected by dc magnetic susceptibility measurements in a SQUID magnetometer (Cryogenic Ltd) with Helium3 insert option. Although sample resistivity was found isotropic at ambient P, the single crystal was thinned down along its naturally grown [111] surface, identified by Laue back-reflection measurement, for high-pressure resistivity and MIR reflectance measurements, to explore possible unusual transport properties in this plane.

High-pressure resistance measurements at low temperature have been performed on a tiny single crystal of 30 μm thick and 100 μm lateral dimension, mounted in a miniature diamond anvil cell (DAC) and with excitation current (10 mA) flowing along the [111] plane. The resistivity was estimated by using the size of the sample at ambient pressure. The standard quasi-four-point contact method was employed using Lakeshore AC370 resistance bridge in combination with fine gold electrodes fabricated on the diamond culet. The sample and electrodes were insulated from the metal gasket using an insulation layer of Al_2O_3 and epoxy mixture, and the sample pressure was measured by the *in situ* ruby luminescence method, as described elsewhere [29]. The pressure difference due to T variation was within 1 GPa at the highest pressure. Finely powdered NaCl has been used as the pressure medium (PTM) and to keep the electrodes in good contact with the sample.

DAC-based high-pressure structural evolution has been studied by monochromatic ($\lambda = 0.68881$ Å) x-ray powder diffraction measurements at the XRD1 beam line of the Elettra synchrotron. A methanol-ethanol-water (MEW; 16:3:1) mixture was used as PTM to provide quasihydrostatic conditions, and gold was used as the pressure marker [30]. The (two-dimensional) 2D diffraction patterns were recorded on a Dectris Pilatus2M detector and these were converted to $I(2\theta)$ diffraction profiles using the FIT2D software. The lattice parameters were determined by means of the Le-Bail profile fitting. Severe inhomogeneity at the high angle diffraction patterns (possibly due to structural disordering) at higher pressures prevents a Rietveld structural analysis. Two measurement runs were performed; run1 up to 50 GPa and run2 up to 15 GPa in finer pressure steps.

Mid-IR reflectance spectra under high pressures have been collected at the SISSI beamline of Elettra synchrotron facility, with the help of an IR microscope (Hyperion) equipped with a liquid-nitrogen-cooled HgCdTe (MCT) detector and coupled to a Bruker IFS66v interferometer. A thin single crystal with a flat [111] surface is placed against the diamond surface in the DAC gasket hole, which is then filled with KCl pressure medium. Reflectance at the sample-diamond interface are measured in the wide frequency range (600–12000 cm^{-1}) up to ∼37 GPa. At each pressure, the intensity of light $I_s(\omega)$ reflected from the sample surface is measured and normalized with the light intensity $I_0(\omega)$ reflected from the external face of diamond window, to obtain a quantity $r(\omega) = \frac{I_s(\omega)}{I_0(\omega)}$. At the end of the pressure run, another measurement is performed on the open diamond surfaces [$I_d(\omega)$,$I_0(\omega)$] by removing the sample. The ratio $R(\omega) = \frac{I_d(\omega)}{I_0(\omega)}$ is assumed to be pressure independent. The reflectance $R_{s-d}(\omega)$ at the sample-diamond interface is thus obtained from the equation $R_{s-d}(\omega) = \frac{r(\omega)}{R(\omega)} R_{\mathrm{dia}}$, where $R_{\mathrm{dia}} = [\frac{n_{\mathrm{dia}}-1}{n_{\mathrm{dia}}+1}]^2$ and n_{dia} is the real refractive index of diamond in air. For accuracy in low-pressure measurements, sufficient initial pressure is applied to keep the sample in good contact with diamond surface. Pressure inside the DAC was monitored by *in situ* ruby luminescence method [31].

III. RESULTS

A. Resistivity under high pressure

High-pressure resistivity data up to 29 GPa from the single-crystal $Cd_2Re_2O_7$ in the temperature range 1.4–300 K are shown in Fig. 1(a). The lowest pressure (0.4 GPa) resistivity exhibits an overall metallic character with distinctive temperature dependencies in different temperature regimes, agreeing well with previous reported data [25]. Although $Cd_2Re_2O_7$ above 340K exhibits a power-law resistivity behavior resulting from the phonon-mediated electron-hole scattering mechanism [21], the present data limited to 300 K show almost linear temperature dependence down to the structural transition at T_{s1}. A relatively high resistivity with almost linear temperature dependence above T_{s1} suggests low carrier density, bad metal character, agreeing with the reported compensated semimetallic band structure for this geometrically frustrated cubic pyrochlore phase [27]. Below T_{s1}, resistivity falls rapidly showing good metal behavior with a subtle signature of another structural transition at T_{s2}. Upon increasing pressure both the structural transitions are suppressed by lowering the transition temperatures and the superconducting transition temperature (T_c) is elevated into the present measurement temperature window. The metallic residual resistivity ρ_0 (ρ right above T_c) rapidly increases with pressure. However, the observed small ρ_0 (~45 $\mu\Omega$cm) at 2.2 GPa indicates good pressure homogeneity as compared to previous reports [24,25]. Pressure-induced rapid increase of ρ_0 indicates high sensitivity of the Fermi surface of the low-temperature tetragonal phase on pressure. As our aim here is to investigate $Cd_2Re_2O_7$ at higher pressures, resistivity measurements have been performed at coarse steps and so we have skipped detailed and subtle resistivity features in the pressure range 3–5 GPa where the system exhibits a large number of electronic phases, as elaborated elsewhere [26]. At higher pressures, the resistivity displays dramatic changes; the cubic pyrochlore undergoes an electronic transition at 8.3 GPa indicated by the sudden change in high-T resistivity behavior and eventually a transition to a nonmetallic state above 21 GPa. A pressure driven metal-nonmetal transition between 21–24 GPa is depicted clearly in resistivity semilog plot in Fig. 1(b).

In Fig. 2 are plotted the resistivity change [$\rho(T)$-ρ_0] as a function of temperature at different pressures. At low temperatures ($T < 15$ K) resistivity follows a quadratic temperature dependence showing Fermi-liquid behavior with electron-electron scattering being the dominant mechanism in the tetragonal phase up to 6.3 GPa [inset of Fig. 2(a)]. The effect of pressure on the low-temperature metallic state up to 4.3 GPa [Fig. 2(a)] is found to agree quite well with the reported results [24,26]. However, no anomalous change in temperature coefficient (A) and ρ_0 is noticed up to 6.3 GPa, unlike the study of Hiroi *et al.* The difference in observed residual resistivity above 4 GPa in various measurements may be attributed to anisotropic resistivity due to local structural anisotropy in the low-temperature tetragonal phase. At 6.3 GPa, linear resistivity is observed down to 100 K where a dip is noticed (shown by down arrow) that may be attributed to a subtle structural transition [26].

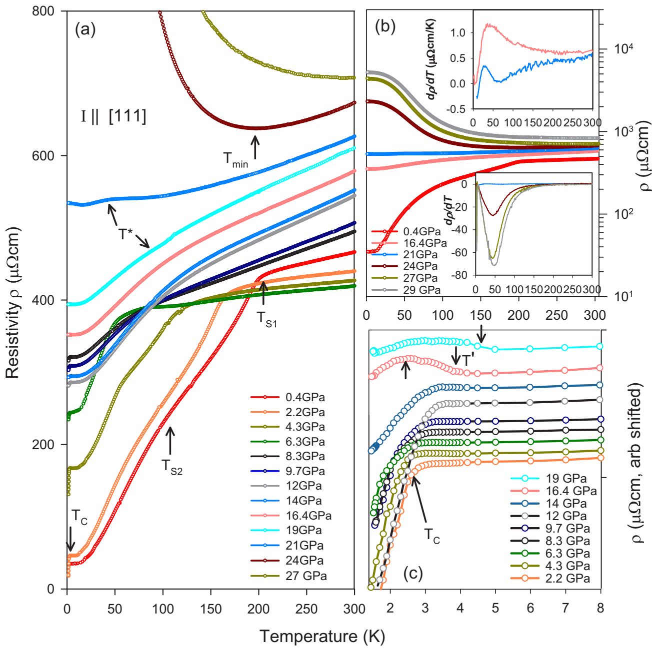

FIG. 1. (a) Resistivity as a function of temperature at various pressures. (b) Resistivity vs temperature plotted on semilog scale for some representative pressures. Insets are the plots of $d\rho/dT$ for the metallic and nonmetallic phases, peaks, and dips indicating transition from high-T incoherent to low-T coherent state. (c) Enlarged view of the resistivity plot around the superconducting transition near 2.5 K at different pressures above 2.2 GPa.

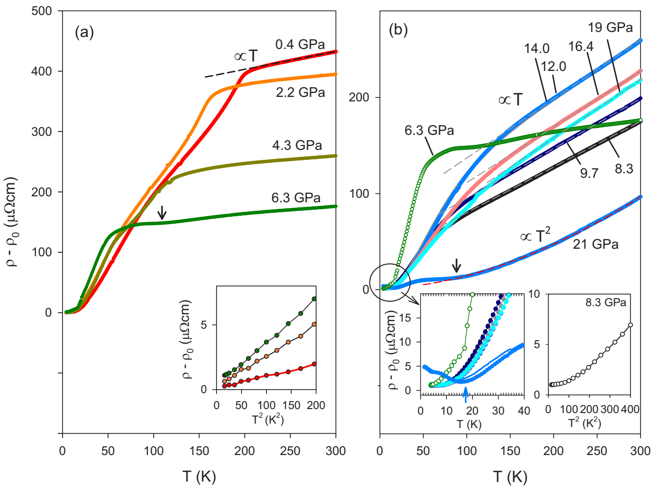

FIG. 2. Plots of relative resistivity (ρ-ρ_0, ρ_0 being the residual metallic resistivity above T_c) as a function of temperature for various high pressures, (a) up to 6.3 GPa and (b) above 6.3 GPa. Enlarged views of low-temperature resistivity as a function of T and T^2 are shown as insets.

The resistivity at 8.3 GPa characterize the metallic cubic pyrochlore phase over the whole temperature range with a large residual resistivity (ρ_0) [24]. The low-temperature resistivity follows T^3 dependence [as shown in right inset of Fig. 2(b)], indicating strong non-Fermi-liquid behavior below ~20 K. A qualitative interpretation of this behavior could be a strong scattering of electrons from the disordered lattice with anomalous lattice vibration even at such a low temperature. With increasing temperature resistivity increases rapidly and approaches a linear T-dependent metallic resistivity, without showing any sign of saturation at 300 K, via a broad crossover temperature (T^*) region indicating a typical strongly correlated metallic character [10,32]. For $T > T^*$, such large metallic resistivity represents incoherent electronic scattering [33,34]. While the metallic resistivity behavior remains unchanged, the overall resistivity increases gradually in the pressure range 8.3–19 GPa.

At 21 GPa, a conspicuous change in resistivity behavior is noticed, with a quadratic power-law temperature dependence ($\rho - \rho_0 = AT^2$ with coefficient $A \sim 10^{-3}$ $\mu\Omega$cm K^{-2} and high residual resistivity $\rho_0 \sim 530$ $\mu\Omega$cm) over a wide temperature range (100–300 K) [Fig. 2(b)]. For $T < 100$ K the metallic resistivity further decreases down to ~17 K with intermediate slope change near 50 K. At further low T the resistivity takes upward turn ($d\rho/dT < 0$), featuring a transition to an unconventional metallic state [shown by up arrow in left inset of Fig. 2(b)]. A clear observation of thermal hysteresis indicates a first-order nature of this transition. At higher pressures (at 24 GPa), $\rho(T)$ increases with decreasing T in a power-law fashion below $T_{\min}$. We will call this state nonmetallic (negative $d\rho/dT$ metal) as the low-temperature resistivity magnitude ($\sim$2 mΩcm) is still low as compared to that of a typical thermally activated insulator [see Fig. 1(b)]. While resistivity upturn below $T_{\min}$ looks Kondo-like as observed in the frustrated Kondo lattice of $Pr_2Ir_2O_7$ [35], a similar effect can be ruled out due to the absence of local f moments in $Cd_2Re_2O_7$ pyrochlore. A similar non-Kondo resistivity upturn has also been reported in the high-pressure nonmetallic state of $Eu_2Ir_2O_7$ [15]. The transition temperature $T_{\min}$ increases rapidly with pressure. An apparent nondivergent resistivity behavior as $T \rightarrow 0$ shows evidence of a novel ground state. A closer look of $\rho(T)$ at low temperature shows a quadratic power-law behavior, indicating validity of Fermi-liquid behavior ($\rho = \rho_0 - A^*T^2$) and therefore the formation of a coherent quasiparticle is also expected in this state. With increasing T, a gradual change in power-law behavior is noticed and the resistivity shows weak T dependence indicating an incoherent state, as discussed for metallic case. The coherent-incoherent crossover (T^*) thus can be clearly identified from the peak (in metal) or dip (in nonmetal) in the $d\rho/dT$ plots [inset of Fig. 1(b)].

Phase diagram

The above results are summarized in the characteristic phase diagram of $Cd_2Re_2O_7$ in Fig. 3(a). The transition temperatures can easily be identified from the derivative ($d\rho/dT$) plot of the resistivity [Fig. 3(c)] [25]. At low pressures ($P < 6.3$ GPa) the derivative plots show a two-peak feature. The sharp peak at T_{s1} corresponds to the reported second-order structural transition. The broader peak at low temperature corresponds to an incoherent to coherent metallic transition (T^*) in the structurally stable low-temperature tetragonal phase emerging at T_{s2}, indicated by the valley between these two peaks. At higher pressures T_{s1}, T_{s2} decrease, revealing the low-temperature behavior of cubic pyrochlore phase. In this state, although low-temperature resistivity behavior remains unchanged [left inset of Fig. 2(b)], high-temperature metallic character changes systematically with the crossover temperature T^* showing an anomalous change near 14 GPa, that may be attributed to the observed second-order structural transition at this P, to be discussed in next section. In Fig. 3(d) are plotted the variation of $d\rho/dT$ at 300 K and the residual resistivity ρ_0 as a function of pressure. Both the quantities show anomalous changes between 6.3–8.3 GPa (P1) and at 14 GPa (P2). Although the initial large increase of ρ_0 with pressure can be attributed to the observed low temperature phase, the observed concurrent change in high-T resistivity slope at P1 evidences an electronic structural change associated with a subtle structural change of the high temperature cubic pyrochlore phase too. As the characteristic temperature T^* scales with inverse of quasiparticle effective mass [10], the above picture indicates a rapid mass enhancement as the system approaches P1, suggesting a quantum critical behavior at this pressure.

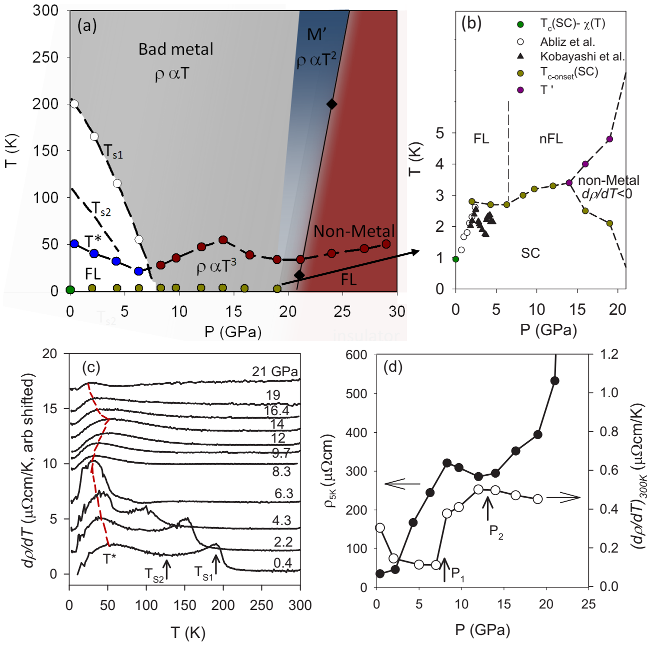

FIG. 3. (a) The phase diagram for pyrochlore $Cd_2Re_2O_7$, constructed from the resistance data. M' indicates the region where T^2-dependent resistivity is observed. (b) Enlarged picture of low-temperature section of the phase diagram; pressure dependence of various transition temperatures, onset superconducting T_c (SC) and emergence of nonmetallic state below T'. (c) Resistivity derivative ($d\rho/dT$) as a function of temperature in the metallic phase up to 21 GPa. Structural transitions are indicated by up arrows and the conherent-incoherent transitions are shown by broken lines. (d) Pressure dependence of the residual resistance (ρ_0) and the linear temperature coefficient at 300 K in the metallic pyrochlore phase.

Another important result is the unusual high-pressure resistivity behavior at low temperature near 3 K. Anomalous resistivity downturn around this temperature is found even up to 19 GPa [see Fig. 1(c)]. In our quasi-four-probe resistance measurements, a nonnegligible gold lead contact resistance does not allow to reach a zero resistance below the superconducting (SC) transition of the sample [24]. For $P > 6.3$ GPa, the broad resistivity drop starts at a higher temperature ($\sim$2.8 K) while maintaining a high resistivity at 1.4 K. While earlier studies have refrained from considering the anomalous resistivity drop above 2.5 GPa as a SC onset [24,36], later hydrostatic pressure measurement evidences the SC transition even up to 4.8 GPa [26]. Therefore the possible sources of nonzero resistivity can be a consequence of large pressure inhomogeneity, sample imperfection or intrinsic anisotropic resistivity. To make a comparison with earlier reported data, we therefore have plotted the pressure dependence of the onset T_c. The onset T_c agrees quite well with the reported data up to 4.3 GPa [26] [see Fig. 3(b)]. Considering the resistivity drop as the onset of SC transition, we conclude that broad transition width at higher pressures is primarily due to the enhanced nonhydrostaticity (due to use of solid pressure medium) as well as intrinsic structural disorder. Our study thus rules out tetragonal distortion as the essential ingredient for the superconducting transition in $Cd_2Re_2O_7$ pyrochlore. However, the origin of superconductivity in the geometrical frustrated ideal cubic pyrochlore phase needs further investigations. It can be noted that a similar resistivity drop in the high-pressure metallic state of Nd$_2$Ir$_2$O$_7$ pyrochlore has been attributed to the weak ferromagnetic spin-ordering transition with frustrated spin-ice-like correlation due to Nd localized f moments [16]. Absence of any localized f moment in Cd$_2$Re$_2$O$_7$ rules out such possibilities. However, we do not have additional information that would elucidate the exact mechanism of this resistivity drop. A magnetoresistance study at high pressure would have been useful to identify any magnetic origin of this resistivity drop. This onset SC transition temperature increases with pressure (3.5 K at 14 GPa). At a further higher pressures (at 16 GPa and 19 GPa) resistivity shows weak upturn below T' ($\sim$4.5 K) forming a peak feature before taking a down turn below 2.5 K. This unconventional metallic feature [$d\rho/dT < 0$, shown by down arrow in Fig. 1(c)] indicates a significant change in the density of states (DOS) at the Fermi energy with possible formation of a pseudogap structure. At 21 GPa, the emergence of a nonmetallic state below 17 K is found to overlap with this phase and so this can be considered as a precursor of high pressure transition to the nonmetallic ground state.

B. X-ray diffraction

Powder diffraction patterns at various high pressures are shown in Fig. 4. The room-temperature cubic pyrochlore phase, which is identified by the single sharp Bragg peaks at 6.5° (111) and at 13.5° (222), is found to be stable up to $\sim$14 GPa, above which each of these peaks starts broadening with emergence of a shoulder peak on the higher angle side. This indicates a structural transition into a low-symmetry phase. Emergence of new peaks without vanishing of any diffraction peak of the cubic phase, is suggestive of a second-order structural transition. From the group-subgroup analysis, the new phase can be indexed as of rhombohedral structure (due to elongation or contraction of a unit cell body diagonal [111] relative to other three body diagonals) with space group $R\bar{3}m$ and $z = 2$. Le-Bail fitted diffraction profiles at 9.5 and 19.9 GPa are shown as inset in Fig. 4. The transformation from the cubic ($Fd\bar{3}m$) to rhombohedral pyrochlore ($R\bar{3}m$) structure is illustrated in Fig. 5(d). The cubic unit cell with lattice parameter a_C can be represented by a rhombohedral unit cell with lattice parameter a_R and α; the two unit cells are related by $a_R = a_C/\sqrt{2}$ and $\alpha = 60°$. When α deviates from 60°, the symmetry reduced from cubic to rhombohedral. The degeneracy of the cubic 111 diffraction peak is removed by splitting into 100 and 111 peak in the rhombohedral phase. The rhombohedral α angle can be easily calculated from the splitting of the cubic 111 or 222 diffraction peaks.

In order to eliminate the possibility of anisotropic broadening due to strong uniaxial stress, cubic phase 111 and 222 diffraction peak widths have been plotted along with Au 111 peak in Fig. 5(c). Apart from the intrinsic differences in the P-dependent peak broadening between 111 and 222 peaks, the peak widths start increasing rapidly above 14 GPa (P_c), suggesting existence of not-well-resolved new shoulder peaks due to the phase transition at this pressure. In Figs. 5(a), 5(b) are plotted the lattice parameters and volume per formula unit as a function of pressure. The rhombohedral distortion may be accounted by the order parameter η ($=\frac{\alpha}{\alpha_0} - 1$), a measure of the deviation of the rhombohedral angle from $\alpha_0 = 60$. Although the lattice parameters show discontinuous changes at 16 GPa (perhaps due to non-well-resolved peaks of the new phase), a negligible volume change confirms a nearly second-order displacive phase transition. This is also apparent from the critical exponent behavior of the order parameter (η) of this phase transition [inset in Fig. 5(a)], with η^2 being the spontaneous lattice strain. The transition pressure P_c, obtained by fitting the equation $\eta = C(P - P_c)^{1/2}$, is 12.5(5) GPa, with $C = 0.0052\mathrm{GPa}^{-1/2}$. The bulk modulus of the cubic pyrochlore phase is found as $B = 137(11)$GPa and $B' = 12(2)$. Cd$_2$Re$_2$O$_7$ is thus found to be relatively soft among all cubic pyrochlore compounds and the only $A_2B_2O_7$ (227) oxide pyrochlore undergoing pressure-induced rhombohedral structural transition. At higher

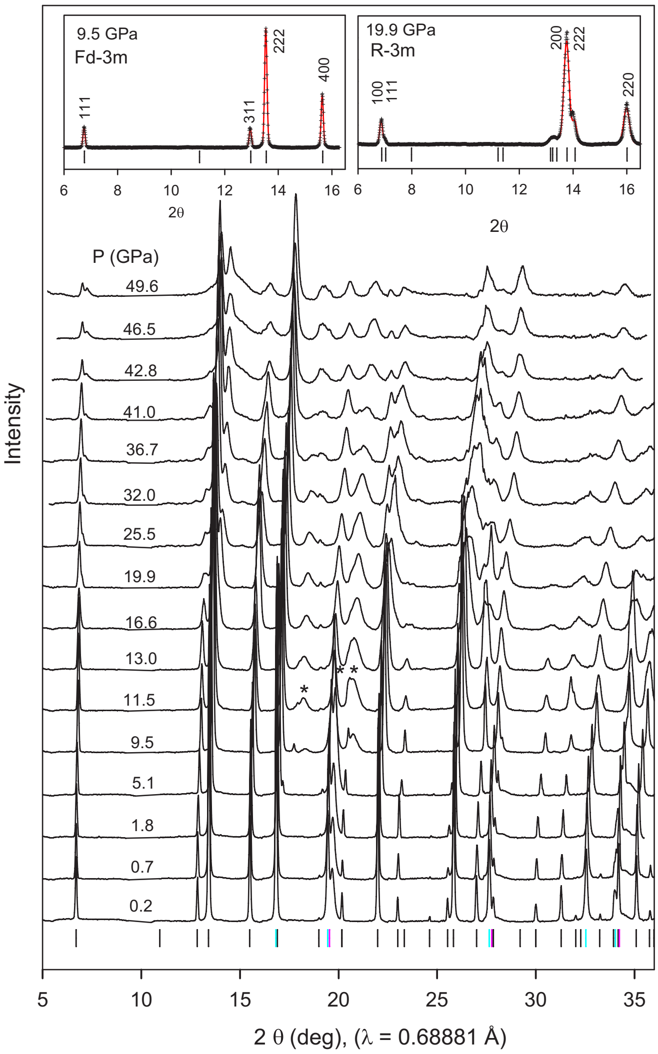

FIG. 4. X-ray diffraction patterns at various high pressures at room temperature. Diffraction peaks marked with vertical bars are Bragg peaks from Cd$_2$Re$_2$O$_7$ (black), Au pressure marker (cyan) and Fe gasket (violet). Above 9.5 GPa, new broad peaks (marked with asterisk) around the Fe peaks correspond to the transformed hcp phase of Fe. Insets show the Le-Bail fitted profile in the cubic and rhombohedral structured pyrochlore phase.

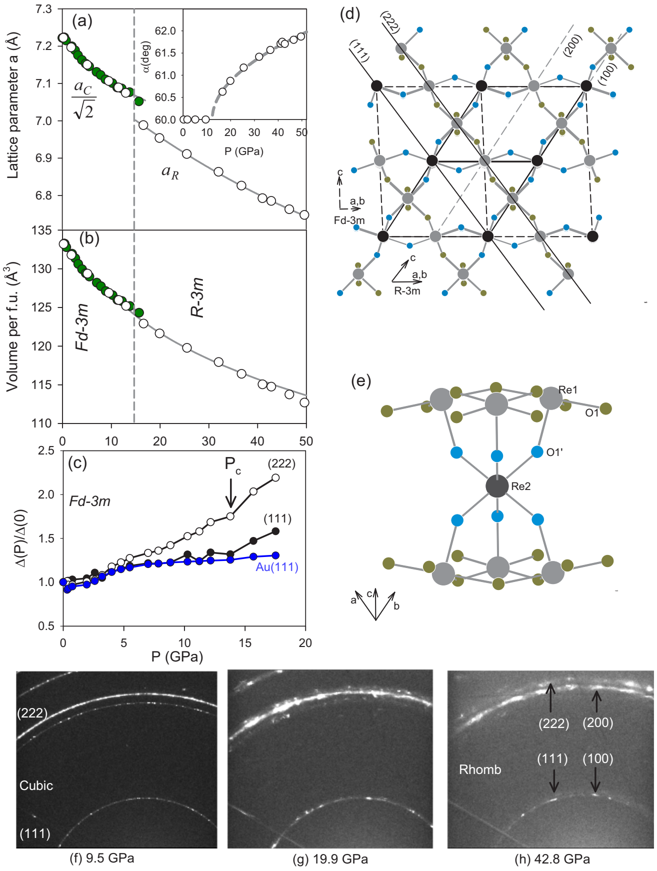

FIG. 5. Variation of (a) lattice constants and (b) volume per formula unit, fitted with third-order Birch Murnaghan equation of state as a function of pressure across the cubic-rhombohedral phase transition at ∼14 GPa. (c) Relative change of peak width of the cubic 111 and 222 Bragg peaks up to the transition pressures as compared with that of Au 111 peak. (d) Structural transformation between the cubic ($Fd\bar{3}m$) and the rhombohedral ($R\bar{3}m$) pyrochlore phase (e) Neighboring Re atoms with different site symmetry (gray and black) in the rhombohedrally distorted pyrochlore structure. The low angle two-dimensional diffraction image of $Cd_2Re_2O_7$ recorded on an area detector at (f) 9.5 GPa (g) 19.9 GPa and (h) 42.8 GPa. Various Bragg peaks are indexed with the cubic and rhombohedral structure.

pressures, particularly in rhombohedral phase 2D diffraction rings become relatively broad and inhomogeneous, with broad patches (spots) on them [Figs. 5(f)–5(h)]. A pressure-induced redistribution of the diffraction intensity suggests a charge redistribution with a probable charge-ordered state, keeping in mind the unconventional oxidation state of the Re^{5+} ion. A high-pressure single-crystal XRD measurement would provide better insight to explore any possible charge ordered state. Beyond 40 GPa, the structure transforms into more disordered state, as seen from the large halo/diffuse scattering. A broad diffusive background in the 2θ range 13–16° indicates admixture of partial disordered state (Fig. 4).

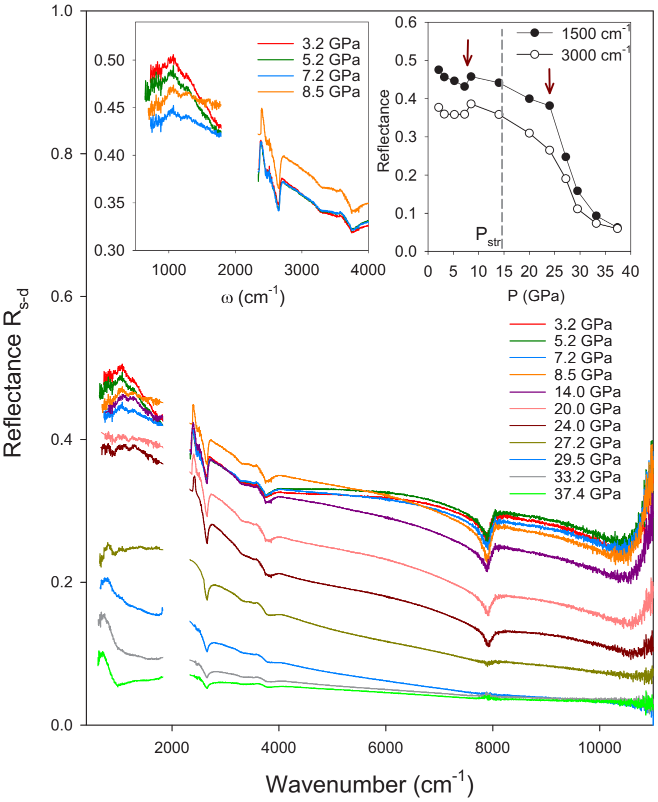

FIG. 6. Reflectance $R_{s\text{-}d}$ at the sample-diamond interface at various pressures up to 37.4 GPa. Left-hand side inset shows an enlarged view of the low-frequency reflectance spectral change up to 8.5 GPa. Right-hand side inset is the plot of reflectance as a function of pressure for two different wave numbers (1500 and 3000 cm^{-1}). The vertical dashed line marks the cubic-rhombohedral transition pressure.

C. High-pressure IR reflectance

The reflectance spectra from $Cd_2Re_2O_7$ single crystal at the sample-diamond interface, $R_{s-d}(\omega)$, at various high pressures are shown in Fig. 6. Strong two-phonon diamond absorption prevents the measurement in the range 1800–2400 cm^{-1}. A reflectivity edge observed around 1.3 eV (∼10500 cm^{-1}) reflects the metallic character of this system. With increasing pressure up to 7.2 GPa, the overall reflectance remains unchanged with only a systematic but small reduction of reflectance in the low-frequency region ($\omega < 1500$ cm^{-1}) (shown as inset of Fig. 6). At higher pressures the spectral feature changes suddenly below 5000 cm^{-1} and the overall reflectance reduces gradually up to 24 GPa. At 27 GPa a drastic change in low-frequency spectra is noticed, with subsequent reduction of reflectance at higher pressures indicating insulating reflectance. However, due to lack of observed FIR reflectance data, a clear Drude reflection is not seen. Pressure dependence of the MIR reflectance at two frequencies (right-hand side inset of Fig. 6) clearly identifies electronic changes near 7 GPa and 24 GPa with strong frequency dependence, while no anomaly is noticed at ∼14 GPa supporting the continuous nature of structural transition at this pressure.

We now turn to the real part of optical conductivity $\sigma_1(\omega)$ of $Cd_2Re_2O_7$, shown in Figs. 7(a), 7(b), as calculated from $R_{s\text{-}d}(\omega)$ by using Kramers-Krönig constrained variational dielectric function analysis [37]. There is large rearrangement of $\sigma_1(\omega)$ across the metal-nonmetal transition above 24 GPa.

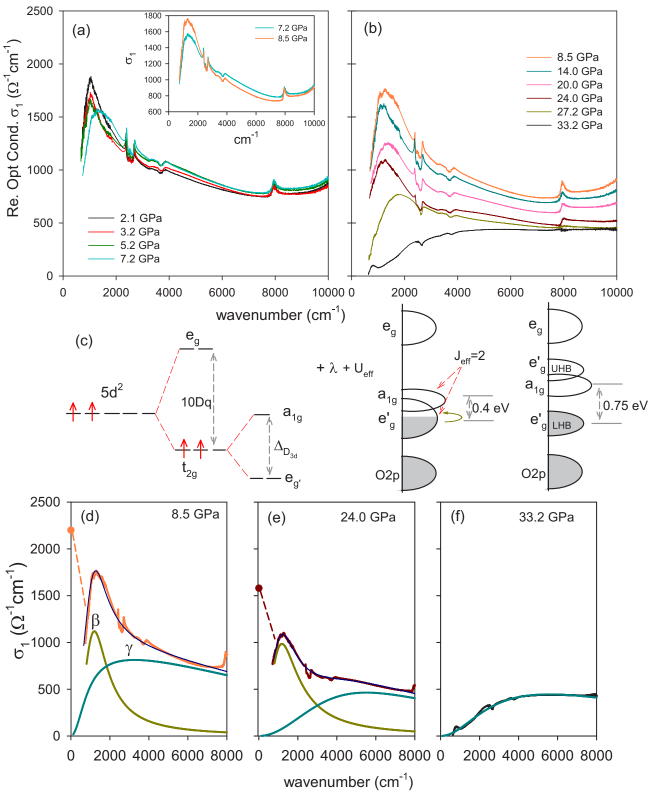

FIG. 7. Pressure-dependent optical conductivity $\sigma_1(\omega)$ at two pressure ranges, (a) $P < 8.5$ GPa and (b) $P > 8.5$ GPa. Inset in (a) shows an enlarged view of spectral weight transfer between 7.2 and 8.5 GPa. (c) A schematic illustration of the Re $5d^2$ electronic states in the $Cd_2Re_2O_7$ pyrochlore structure. The Drude part in the metallic phase originating from the intraband transition and the MIR band originating due to transitions between e_g' and a_{1g} sub-bands in presence of SOC (λ) and effective electronic correlation (U_{eff}). (d) Drude-Lorentz fit of the optical conductivity at (d) 8.5 GPa, (e) 24 GPa, and (f) 33.2 GPa. σ_{dc} ($=\frac{1}{\rho_{dc}}$) is plotted at $\omega = 0$ and a dashed line is drawn from the lowest measured $\sigma_1(\omega)$ to indicate Drude features.

The low-pressure $\sigma_1(\omega)$ in the spectral range 700–8000 cm^{-1} comprises of a strong Drude-like low-frequency feature with a peak structure at 1000 cm^{-1} ~ 0.12 eV (a signature of incoherent carrier transport) and a MIR band with peak energy at 3200 cm^{-1} ($\sim$0.4 eV), agreeing with the reported results [38]. Incoherent quasiparticle dynamics gives rise to broad Drude-like feature at finite energy, as reported for the incoherent metallic LiV_2O_4 with pyrochlore lattice structure [34]. Up to 7.2 GPa, the overall $\sigma_1(\omega)$ spectra remains mostly unchanged, with slight decrease of the low-frequency peak intensity with associated peak broadening. At 8.5 GPa we noticed a sudden SW transfer from MIR to FIR region around 3000 cm^{-1} (isosbestic point) [see inset of Fig. 7(a)]. This agrees well with the observed resistivity anomaly at 8.3 GPa. An enhanced finite energy Drude SW with reduced dc conductivity at 8.5 GPa can be understood in terms of higher incoherent scattering, possibly of larger intrinsic lattice disorder. This is further supported from the observed non-Fermi-liquid low-T resistivity behavior above this pressure. The $\sigma(\omega)$ at higher pressures have been plotted in Fig. 7(b). With increasing pressure above 8.5 GPa, the overall spectral weight rapidly decreases. Simultaneous gradual reduction of dc conductivity (as seen in resistivity data) implies that the SW must have transferred beyond this measurement energy range, featuring involvement of high-energy interband transitions, a common phenomena of correlated electron systems. However, Coulomb correlation ($U \sim$ 1-2 eV) is found to have a little effect on the cubic phase Re t_{2g} bands in presence of strong spin-orbit interaction [39]. At 27.2 GPa, an abrupt change in the low-frequency spectral feature is seen with possible gap structure. However, based on the observed dc conductivity ($\sim$1000 $\Omega^{-1}\text{cm}^{-1}$) we can say that it arises either due to incomplete gap opening at the Fermi surface (semimetallic character) or the formation of pseudogap structure at the Fermi level, causing a metal-nonmetal transition. In order to understand the band structure changes in more detail across this transition, $\sigma_1(\omega)$ has been fitted with Drude-Lorentz oscillators [Figs. 7(d)–7(f)].

Metal to nonmetal transition

The photoemission data and band structure calculations on cubic pyrochlore $Cd_2Re_2O_7$ have shown that the active bands close to the Fermi level arise from the Re t_{2g} states [39–41]. These are well separated from the Re e_g, O $2p$, and Cd $5s$ bands and so Re-Re intersite transitions between t_{2g} to e_g and charge transfer between O_{2p} to t_{2g} or t_{2g} to Cd $5s$ are expected to occur in the optical conductivity spectra above $\sim$4 eV [38]. Therefore, the present optical conductivity spectra measured up to 10000 cm^{-1} (=1.24 eV) can be explained in terms of various intra-t_{2g} transitions. At ambient pressure cubic phase, local trigonal crystal field (Δ_{D3d}) arising from the elongated ReO_6 octahedra (due to $x < x_c$) lifts the t_{2g} level degeneracy into a singlet a_{1g} and a lower-lying doublet e_g' bands [7,13,42]. Although from the LDA calculation a_{1g} band is found much narrower compared to e_g' band, two electrons are partially shared among these two bands. In Fig. 7(c), the schematic energy level diagram for the $5d^2$ electron states has been described assuming a simple two-band model (a_{1g}, e_g') for t_{2g} states in presence of effective electronic correlation (U_{eff}) to explain the observed two-band feature of $\sigma_1(\omega)$. Unlike iridate pyrochlore compounds, because of d^2 electronic configuration these bands comprise of $J_{\text{eff}} = 2$ character multiplets due to strong spin-orbit interaction (λ), making $\sigma_1(\omega)$ analysis more complicated. However, the above simple picture will help understand the pressure-induced metal to nonmetal transition.

The low-pressure $\sigma_1(\omega)$ in the spectral range 700–8000 cm^{-1} are very well fitted with two Lorentz oscillators [β and γ, as shown in Fig. 7(d)]. The sharp peak β at $\sim$1000 cm^{-1} ($\sim$120 meV) is assigned as incoherent part of the Drude conductivity (as discusses above), originating from intra-e_g' transitions. A linear extrapolation matches well the dc conductivity ($\sigma_{dc} = 1/\rho_{dc}$). The broad band at 3200 cm^{-1} ($\sim$0.4 eV) corresponds to $e_g' \Rightarrow a_{1g}$ transition. This matches well with the crystal field splitting (Δ) in various $5d$ pyrochlores and of the same order ($\sim$0.4 eV) as the spin-orbit interaction (λ) [14]. As P increases through the structural transition at 14 GPa, the overall $\sigma_1(\omega)$ decreases systematically with major changes occurring in the γ band as its peak energy increases. As the γ-band energy here is a measure of effective trigonal crystal field splitting (Δ_{D3d}), including trigonal lattice distortion in the rhombohedral phase, an enhanced crystal field energy ($\Delta = 0.75$ eV) is observed at 24 GPa. With $\Delta > \lambda$, the half-filled e_g' band becomes more susceptible to be controlled by the strong electronic correlation. At 27 GPa, a dramatic change in the $\sigma_1(\omega)$ is noticed with rapid decrease of the β band intensity and so the incoherent Drude part vanishes. This may be viewed as the Mott transition of the e_g' band, opening a Mott gap [shown schematically in Fig. 7(c)]. The γ band in the Mott insulating state corresponds to the transition between e_g'-LHB to a_{1g}. However a large dc conductivity indicates nonzero DOS at the Fermi level. As a result of large bandwidth, the filled e_g'-LHB band overlaps with almost unoccupied a_{1g}, a semimetallic state perhaps emerges. The e_g'-LHB to UHB transition band is expected to appear beyond this measurement range and so U_{eff} cannot be estimated from this study.

IV. DISCUSSION

We start our discussion with the important observation at 21 GPa of the unusual resistivity behavior in the rhombohedral pyrochlore phase. In this phase, Re occupies two different site symmetry positions [Re1, Re2, as shown in Fig. 5(d)]. With large trigonal lattice distortion, the Re1-Re1 distance increases with respect to Re1-Re2. The system looks like a quasi-2D Kagome lattice with geometrical frustration maintaining in the [111] plane, while this is suppressed in the perpendicular plane. With unequal nearest-neighbor hopping amplitude, the system approaches a nonmetallic ground state, as predicted for pyrochlore iridates in Ref. [7]. The rapid evolution of the Fermi surface at this transition boundary is reflected from the conspicuous change of temperature dependence of metallic resistivity. A quadratic power law at high temperature implies predominant strong electron-electron scattering at this pressure. Moreover, the large nonsaturated resistivity at 300 K indicates correlated electron behavior. A drastic reduction of the incoherent Drude peak (β) in the optical conductivity further supports this behavior. A first-order nature of the metal-nonmetal transition below T_{min} thus indicates that the system approaches a Mott-type metal to insulator transition. This is also supported from the fact that T_{min} emerges almost from $T = 0$ with large P dependence. However, at the transition boundary, the Mott physics here is finely controlled by the large spin-orbit interaction. A finite metallic resistivity as $T \rightarrow 0$ arises from small intrinsic Fermi pockets or surface states characteristic of topological insulators. The low-T resistivity behavior is also found to be similar to the calculated resistivity for Weyl semimetal state of $Y_2Ir_2O_7$ pyrochlore [43].

At higher pressures ($P > 24$ GPa), the nondivergence of resistivity as $T \rightarrow 0$ may be thought as due to bulk impurity states. However, the exact role of disorder in Mott insulating phase is not clear. As the low-pressure tetragonal distortion in pyrochlore makes the system good metallic, a disorder-driven Anderson localization can be ruled out in the high-pressure rhombohedral pyrochlore structure. Valence disproportion-induced charge ordering insulating state in the rhombohedral phase would have displayed thermally activated resistive behavior. However, the role of charge/orbital fluctuation at low temperature in this phase cannot be ruled out for the emergence of the unusual nonmetallic state. Here, we speculate that the large trigonal lattice distortion-induced electron-lattice coupling in competition or cooperation with spin-orbit coupling modifies the band structure by narrowing their bandwidth and lifting a_{1g} band at higher level. The doubly degenerate e_g' band becomes eventually half filled satisfying the Mott criteria to undergo bandwidth controlled correlation-driven metal-nonmetal transition. The metallic phases in the vicinity of localization transitions are usually subject to strong fluctuations in the spin, charge, and orbital degrees of freedom, resulting in unconventional transport properties. A quadratic power-law behavior with large resistivity at 21 GPa (even up to 300 K) and coherent Fermi-liquid behavior (at $T \rightarrow 0$) in the high-pressure nonmetallic state are examples of such physics.

The nature of insulating phase is of tremendous interest due to theoretical prediction of possible novel nontrivial topological state in pyrochlore lattice. A partially suppressed geometrical frustration is found as the key ingredient for the emergence of novel ground state. This general scenario may be extended to isostructural osmate pyrochlore too. In absence of any direct measurement procedure at high pressure (resistivity being the bulk state measurement technique, not the surface states), a model calculation based on our observed structural parameters will help understand this novel phase, especially the role of e_g-t_{2g} and Cd 5s-Re t_{2g} hybridization. From an experimental point of view, in order to gain further insight of the nonmetallic phase, we plan for magnetoresistance and Hall measurements on $Cd_2Re_2O_7$ at high pressures.

V. CONCLUSION

To summarize, a combined high-pressure structural, electrical resistivity, and optical conductivity measurements have been performed to understand the electronic changes with structural evolution in pyrochlore $Cd_2Re_2O_7$. High-temperature cubic pyrochlore phase (SG: $Fd\bar{3}m$) undergoes a second-order structural transition with trigonal distortion in its pyrochlore lattice (SG: $R\bar{3}m$) at ~14 GPa. In the high-pressure rhombohedral phase, the resistivity at high temperature shows a distinct transition at 21 GPa from incoherent metallic (phonon scattering dominated linear T-dependent) to heavy mass Fermi liquid (T^2-dependent) character. Subsequently, a thermally driven metal-to-nonmetal transition is observed at T_{min} that gradually increases with pressure, contrary to Ir-, Os-, and Ru-based 227 pyrochlore compounds. High-pressure optical conductivity measurement on the [111] surface suggests a correlation-driven mechanism of this transition as crystal field exceeds spin-orbit interaction due to large structural distortion. A partial suppression of geometrical frustration might have played important role. Our results have important implication for the possible realization of the distortion driven nontrivial topological insulating state in any 5d pyrochlore that needs further investigation both by theory and experiment.

ACKNOWLEDGMENTS

We thank A. K. Mishra, N. N. Patel, M. Polentarutti, and A. Perucchi for their support during XRD and IR measurements at the Elettra Sincrotrone Trieste. Financial support by the

Department of Science and Technology (Government of India) and ICTP (Italy) are gratefully acknowledged. We would like to acknowledge A. Thamizhavel for helping determine the crystal orientation by Laue back-reflection measurement.

[1] B. J. Kim, H. Jin, S. J. Moon, J.-Y. Kim, B.-G. Park, C. S. Leem, J. Yu, T. W. Noh, C. Kim, S.-J. Oh *et al.*, Phys. Rev. Lett. **101**, 076402 (2008).
[2] S. J. Moon, H. Jin, K. W. Kim, W. S. Choi, Y. S. Lee, J. Yu, G. Cao, A. Sumi, H. Funakubo, C. Bernhard *et al.*, Phys. Rev. Lett. **101**, 226402 (2008).
[3] M. A. Subramanian, G. Aravamudan, and G. V. S. Rao, Prog. Solid State Chem. **15**, 55 (1983).
[4] J. E. Greedan, J. Mater. Chem. **11**, 37 (2001).
[5] S. Fujimoto, Phys. Rev. Lett. **89**, 226402 (2002).
[6] H.-M. Guo and M. Franz, Phys. Rev. Lett. **103**, 206805 (2009).
[7] B.-J. Yang and Y. B. Kim, Phys. Rev. B **82**, 085111 (2010).
[8] L. Hozoi, H. Gretarsson, J. P. Clancy, B.-G. Jeon, B. Lee, K. H. Kim, V. Yushankhai, P. Fulde, D. Casa, T. Gog *et al.*, Phys. Rev. B **89**, 115111 (2014).
[9] D. Uematsu, H. Sagayama, T. H. Arima, J. J. Ishikawa, S. Nakatsuji, H. Takagi, M. Yoshida, J. Mizuki, and K. Ishii, Phys. Rev. B **92**, 094405 (2015).
[10] N. Takeshita, C. Terakura, Y. Tokura, A. Yamamoto, and H. Takagi, J. Phys. Soc. Jpn. **76**, 063707 (2007).
[11] K. Matsuhira, M. Wakeshima, R. Nakanishi, T. Yamada, A. Nakamura, W. Kawano, S. Takagi, and Y. Hinatsu, J. Phys. Soc. Jpn. **76**, 043706 (2007).
[12] D. Mandrus, J. R. Thompson, R. Gaal, L. Forro, J. C. Bryan, B. C. Chakoumakos, L. M. Woods, B. C. Sales, R. S. Fishman, and V. Keppens, Phys. Rev. B **63**, 195104 (2001).
[13] M. Hanawa, Y. Muraoka, T. Tayama, T. Sakakibara, J. Yamaura, and Z. Hiroi, Phys. Rev. Lett. **87**, 187001 (2001).
[14] W. Witczak-Krempa and Y. B. Kim, Phys. Rev. B **85**, 045124 (2012).
[15] F. F. Tafti, J. J. Ishikawa, A. McCollam, S. Nakatsuji, and S. R. Julian, Phys. Rev. B **85**, 205104 (2012).
[16] M. Sakata, T. Kagayama, K. Shimizu, K. Matsuhira, S. Takagi, M. Wakeshima, and Y. Hinatsu, Phys. Rev. B **83**, 041102 (2011).
[17] H. Shinaoka, T. Miyake, and S. Ishibashi, Phys. Rev. Lett. **108**, 247204 (2012).
[18] J. Yamaura, K. Ohgushi, H. Ohsumi, T. Hasegawa, I. Yamauchi, K. Sugimoto, S. Takeshita, A. Tokuda, M. Takata, M. Udagawa *et al.*, Phys. Rev. Lett. **108**, 247205 (2012).
[19] N. A. Bogdanov, R. Maurice, I. Rousochatzakis, J. van den Brink, and L. Hozoi, Phys. Rev. Lett. **110**, 127206 (2013).
[20] S. Calder, J. G. Vale, N. A. Bogdanov, X. Liu, C. Donnerer, M. H. Upton, D. Casa, M. D. Lumsden, Z. Zhao, J.-Q. Yan *et al.*, arXiv:1508.01848.
[21] J. He, D. Hitchcock, I. Bredeson, N. Hickman, T. M. Tritt, and S. N. Zhang, Phys. Rev. B **81**, 134302 (2010).
[22] J.-I. Yamaura and Z. Hiroi, J. Phys. Soc. Jpn. **71**, 2598 (2002).
[23] R. Jin, J. He, J. R. Thompson, M. F. Chisholm, B. C. Sales, and D. Mandrus, J. Phys.: Condens. Matter **14**, L117 (2002).
[24] Z. Hiroi, T. Yamauchi, T. Yamada, M. Hanawa, Y. Ohishi, O. Shimomura, M. Abliz, M. Hedo, and Y. Uwatoko, J. Phys. Soc. Jpn. **71**, 1553 (2002).
[25] N. Barisic, L. Forro, D. Mandrus, R. Jin, J. He, and P. Fazekas, Phys. Rev. B **67**, 245112 (2003).
[26] T. C. Kobayashi, Y. Irie, J. Yamaura, Z. Hiroi, and K. Murata, J. Phys. Soc. Jpn. **80**, 023715 (2011).
[27] Z. Hiroi, M. Hanawa, Y. Muraoka, and H. Harima, J. Phys. Soc. Jpn. **72**, 21 (2003).
[28] I. A. Sergienko, V. Keppens, M. McGuire, R. Jin, J. He, S. H. Curnoe, B. C. Sales, P. Blaha, D. J. Singh, K. Schwarz *et al.*, Phys. Rev. Lett. **92**, 065501 (2004).
[29] S. Karmakar, High Press. Res. **33**, 381 (2013).
[30] A. Dewaele, P. Loubeyre, and M. Mezouar, Phys. Rev. B **70**, 094112 (2004).
[31] H. Mao, J. Xu, and P. Bell, J. Geophys. Res. **91**, 4673 (1986).
[32] C. Urano, M. Nohara, S. Kondo, F. Sakai, H. Takagi, T. Shiraki, and T. Okubo, Phys. Rev. Lett. **85**, 1052 (2000).
[33] M. Tachibana, Y. Kohama, T. Shimoyama, A. Harada, T. Taniyama, M. Itoh, H. Kawaji, and T. Atake, Phys. Rev. B **73**, 193107 (2006).
[34] P. E. Jonsson, K. Takenaka, S. Niitaka, T. Sasagawa, S. Sugai, and H. Takagi, Phys. Rev. Lett. **99**, 167402 (2007).
[35] S. Nakatsuji, Y. Machida, Y. Maeno, T. Tayama, T. Sakakibara, J. van Duijn, L. Balicas, J. N. Millican, R. T. Macaluso, and J. Y. Chan, Phys. Rev. Lett. **96**, 087204 (2006).
[36] M. Abliz, M. Hedo, Z. Hiroi, T. Matsumoto, M. Hanawa, and Y. Uwatoko, J. Phys. Soc. Jpn. **72**, 3039 (2003).
[37] A. B. Kuzmenko, Rev. Sci. Instrum. **76**, 083108 (2005).
[38] N. L. Wang, J. J. McGuire, T. Timusk, R. Jin, J. He, and D. Mandrus, Phys. Rev. B **66**, 014534 (2002).
[39] S.-W. Huang, H.-T. Jeng, J.-Y. Lin, W. J. Chang, J. M. Chen, G. H. Lee, H. Berger, H. D. Yang, and K. S. Liang, J. Phys.: Condens. Matter **21**, 195602 (2009).
[40] D. J. Singh, P. Blaha, K. Schwarz, and J. O. Sofo, Phys. Rev. B **65**, 155109 (2002).
[41] H. Harima, J. Phys. Chem. Solids **63**, 1035 (2002).
[42] M. M. Qazilbash, A. A. Schafgans, K. S. Burch, S. J. Yun, B. G. Chae, B. J. Kim, H. T. Kim, and D. N. Basov, Phys. Rev. B **77**, 115121 (2008).
[43] P. Hosur, S. A. Parameswaran, and A. Vishwanath, Phys. Rev. Lett. **108**, 046602 (2012).